Copyright © 2014 Tech Science Press FDMP, vol.10, no.4, pp.503-520, 2014

Heat Transfer Related to a Self-Sustained Oscillating Plane Jet Flowing Inside a Rectangular Cavity

F. Iachachene[1], **A. Matoui**[2] **and Y. Halouane**[1]

Abstract: Computations related to a heat transfer and fluid flow of a plane isothermal fully developed turbulent plane jet flowing into a rectangular hot cavity are reported in this paper. Both velocity and temperature distributions are computed by solving the two-dimensional Unsteady Reynolds Averaged Navier–Stokes (URANS) equations. This approach relies on one point statistical modeling based on the energy - specific dissipation (k-ω) turbulence model. The numerical simulations are carried out in the framework of a finite volume method. This problem is relevant to a wide range of practical applications including forced convection and the ventilation of mines, enclosure or corridors. The structural properties of the flow and heat transfer are described for several conditions. An oscillatory regime is evidenced for particular jet location, inducing for each variable a periodic behavior versus time. The jet flapping phenomena is detailed numerically through the instantaneous streamlines contours and the vorticity magnitude contours within one period of oscillation. The heat transfer along the cavity walls is also periodic. Time average of mean Nusselt number is correlated with some problem parameters.

Keywords: Impinging jet, Nusselt number, self-oscillation, turbulence, cavity.

Nomenclatures

H	Height of the jet exit [m]
h_0	Nozzle thickness [m]
k	Turbulent kinetic energy [m^2s^{-2}]
L_f	Non-dimensional impinging distance (= X/h_0)
L_h	Non-dimensional jet height (= H/h_0)
Nu(x,t)	Instantaneous local Nusselt number

[1] Department of energetic, faculty of Physics University M'hamed Bouguerra Boumerdes UMBB, Boumerdes, Algeria.
[2] Theoretical and applied laboratory of fluid mechanics, University of sciences and Technology Houari Boumedienne - USTHB.

Nu_L	Local Nusselt number on the lower wall
Nu_B	Nusselt number on the bottom wall
Nu_u	Nusselt number on the upper wall
$\overline{Nu_{cavity}}$	Average Nusselt number on the the three walls
P	Mean pressure [Pa]
P_r	Prandlt number
$R_e = \frac{U_0 h_0}{v}$	Reynolds number
T	Mean temperature
T_w	Wall temperature
U	Axial mean velocity
V	Radial mean velocity
U_0	Jet exit mean velocity
$\overline{u_i u_j}$	Reynolds stress component [$m^2 s^{-2}$]
x, y	Streamwise and transverse coordinate
X	location of the jet exit

Greek symbols

ε	Dissipation of turbulent energy [$m^2.s^{-3}$]
ρ	Fluid density [Kgm^{-3}]
μ	Turbulent eddy viscosity [$Kg.m^{-1}.s^{-1}$]
ω	Specific dissipation rate [s^{-1}]
v	Kinematic viscosity

Subscript

in	initial
t	Turbulent
w	wall

1 Introduction

Heat transfers by impinging jets are found in many engineering applications, such as: cooling of turbine blades, tempering of glassware, drying of paper or textile, etc. The knowledge about the local heat transfer coefficient distribution on the impinging wall is very important for the control processes in any of these applications to obtain high-quality products. Many publications are found in the available scientific literature [Martin (1977); Li and Tao (1993); Brignoni and Garimella (2000);

Chanet al. (2002); Zidouni et al. (2009); Mahrouche et al. (2013); Benmouhoub and Mataoui (2013); Halouane et al. (2013)], have confirmed the dependence of the heat transfer with some number of parameters, such as Reynolds number, temperature, the impinging distance , the lateral confining wall and the nozzle shape. The present work reports computations of the fluid flow and thermal fields for plane isothermal fully developed turbulent jet issuing into a rectangular hot cavity (figure1).

Many researchers [Ogab(1985); Shakouchi et al. (1986); Mataoui and Schiestel (2009)] shown that, when the jet is set in the mid-plane of a cavity, an oscillatory flow occurs.

These self-sustained oscillations are generated by an instability produced by the configuration of a plane jet located between two symmetrical lateral vortices .For non-symmetrical case of the jet location in the cavity, the same phenomenon occurs and sometimes is reinforced [Mataoui et al. (2001)]. A combined numerical and experimental investigation of flow fields and the thermal process of the connected channels are performed by Amon et al. (1992) to gain insight into the operation of compact surfaces of the heat exchangers equipped with the partitioned plates. It has been shown that communicating channels composed of interrupted surfaces offer important heat transfer performance advantages over plane channels. They generate thinner thermal boundary layers as well as enhance mixing due to self-sustained oscillation. In the same topic some numerical investigations of the flow structure and those of the heat transfer in a channel with periodically mounted transverse vortex generators (bars) have been conducted by Valencia (1999). Due of the self-sustained oscillations of the rate of heat transfer is significantly enhanced confirming that this geometry is appropriate for compact heat exchangers. Recently, pulsed impinging jets have received increasing interests while they are widely used to increase heat transfer [Kim (2012); XU et al. (2010)].

This study extends the previous work of Mataoui et al. (2009) and (2001) by considering heat transfer effects on oscillatory regime. The effects of Reynolds number and jet location on local Nusselt number for each cavity wall are examined. The phenomenon is unsteady under some conditions [Mataoui et al. (2001)] and the flow fields are found in good agreement with available experimental data.

2 Methodology

2.1 Governing equations

The numerical study is carried out using URANS turbulence modeling. The fluid is assumed Newtonian and incompressible with constant thermo physical properties. The URANS equations for incompressible flow in Cartesian coordinates are

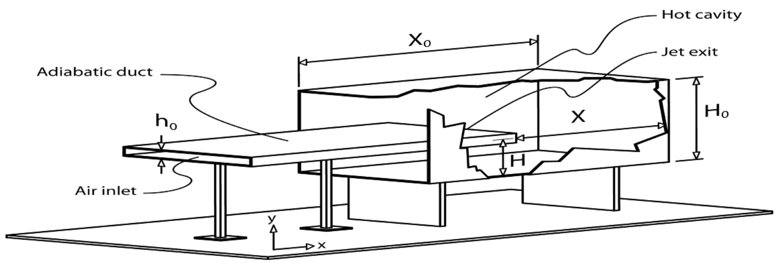

Figure 1: Configuration, jet hot cavity interaction.

deduced from the mass, momentum and energy balance equations coupled with the equations of the turbulent quantities as follows:

Mass conservation equation:

$$\frac{\partial U_i}{\partial x_i} = 0 \tag{1}$$

Momentum conservation equation:

$$\rho \frac{\partial U_i}{\partial t} + \rho U_j \frac{\partial U_i}{\partial x_j} = -\frac{\partial P}{\partial x_i} + \frac{\partial}{\partial x_j}\left(\mu \frac{\partial U_i}{\partial x_j} - \rho \overline{u_i u_j}\right) \tag{2}$$

Energy conservation equation:

$$\rho \frac{\partial T}{\partial t} + \rho U_i \frac{\partial T}{\partial x_i} = \frac{\partial}{\partial x_i}\left(\frac{\mu}{p_r}\frac{\partial T}{\partial x_i} - \rho \overline{u_i \theta}\right) \tag{3}$$

Where P, T and U_i are the mean pressure, temperature and velocity components respectively, θ and u_i are the temperature fluctuation and velocity components fluctuations, respectively; x_i is the space coordinates, t is the time, and ρ, μ, Pr are respectively the fluid density, dynamic viscosity and Prandtl number.

2.2 Turbulence modeling

In the URANS equations, the Reynolds stress component $\overline{u_i u_j}$ and correlations between the velocity and temperature fluctuations $\overline{u_i \theta}$ require modeling. Those are deduced by the following algebraic equations which based on Boussinesq assumption:

$$\overline{u_i u_j} = \frac{2}{3} k \delta_{ij} - \nu_t (U_{i,j} + U_{j,i}) \tag{4}$$

$$-\rho \overline{u_i \theta} = \alpha_t \frac{\partial T}{\partial x_i} \tag{5}$$

By analogy with molecular transport, the turbulent Prandtl number for energy transport equation is determined by Equation 6:

$$\sigma_T = \frac{\mu_t}{\alpha_t} \tag{6}$$

The one-point closure turbulent models are based on the concept of Prandtl-Kolmogorov's turbulent viscosity. In this paper, the closure of the equations is achieved using the SST energy- specific dissipation rate (k-ω) turbulence model. One of the advantages of the SST k-ω formulation is the low-Reynolds number modeling prediction necessary close to the wall. The procedure of the SST model is to use a k-ω formulation in the inner part of the boundary layer and the k-ε model in the outer part of the boundary layer. To combine these two models together, the standard k-ε model is transformed into equations based on k and ω, which leads to the introduction of a cross-diffusion term in dissipation rate equation [Menter (1994); Wilcox (1994)].The near-wall mesh, must be fine in order to resolve the laminar sub-layer. A detailed description of this model is presented in Menter (1994), Wilcox (1994) and ANSYS14 Documentation.

2.3 Numerical procedure

The numerical predictions carried out by finite volume method (Patankar, S.V. 1980) are realized by the ANSYS FLUENT 14.0 CFD code. The spacial discretization of each transport equation is achieved on collocated meshes (ANSYS 14 Documentation). The convection-diffusion terms are interpolated using the POWER LAW scheme for U, V, k, ω and T and second order scheme for the pressure .The pressure-velocity coupling is achieved by SIMPLE algorithm. The solution is considered converged when the normalized residual of each variable reach 10^{-6}. Furthermore, internal iterations are achieved within each time step to resolve the time non-linearity of the equations. To detect the flow regime, unsteady computations are performed for all cases. The time average of the instantaneous values is deduced by a post processing treatment. The transport equation for two dimensional in Cartesian coordinate of dynamical and thermal characteristics of mean and turbulent flow required for finite volume method is:

$$\frac{\partial}{\partial t}(\rho\varphi) + \frac{\partial}{\partial x_j}(\rho U_i \varphi) = \frac{\partial}{\partial x_j}\left[\Gamma_\varphi \frac{\partial \varphi}{\partial x_j}\right] + S_\varphi \tag{7}$$

Where φ is one of the dependent variables U, V, T, k and ω, Γ_φ and S_φ are the corresponding diffusion coefficient and source terms of each equation respectively.

Figure 2 reports the dynamical, thermal and geometrical conditions of the present study.

Constant values of inlet boundary conditions are imposed as follow: $U = U_0, V = 0$, $k_0 = 0.03U_0^2$, $\varepsilon_0 = \frac{k_0^{3/2}}{\lambda h_0}$ $(\lambda = 0.1)$, $\omega_0 = \frac{1}{c_\mu}\frac{\varepsilon_0}{k_0}$, $T = T_0$.

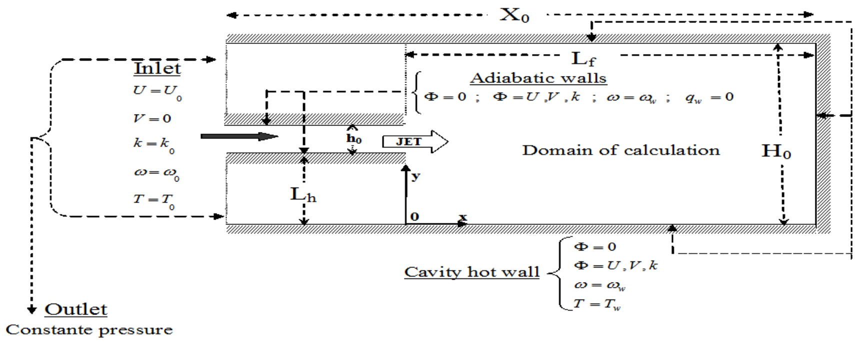

Figure 2: Boundary conditions and parameters.

For each wall, the velocity components (U and V) and kinetic energy (k) are set to zero and the specific of dissipation rate ω is set to asymptotic value proposed by Wilcox (1994). For temperature, the cavity walls are heated and kept at constant value T_w, ($T_w > T_0$). The duct walls are adiabatic. Geometrical and dynamical parameters considered in different computational simulations are given in Table 1.

Table 1: Summary of the simulation conditions.

h_0	H_0	X_0	L_f	L_h	T_0	T_w	Re
1cm	20cm	50cm	$25 \leq L_f \leq 40$	$8.5 \leq L_h \leq 10$	300 K	360k	$2600 \leq Re \leq 8000$.

The OUTFLOW (fully developed) boundary conditions were used. Constant relative static pressure kept at atmospheric level.

A structured mesh composed of non-uniform cells is used. A refinement before and after the outlet of the nozzle are achieved so that the entrainment of the flow is described with good accuracy. Sufficiently fine grids are adopted in the viscous sub-layer, near each wall where a very high gradient of variables prevail (Figure3). For each interaction case a grid independency test is carried out by refining and adjusting the grid in the two directions.

Figure 4 shows the effect of grid size on the average Nusselt number distribution on the bottom wall and the average axial mean velocity $\bar{U}$ on a long line ($x/h_0=10$), for the jet-cavity interaction $L_f=25$ and $L_h=10$. It is observed that grid independence is

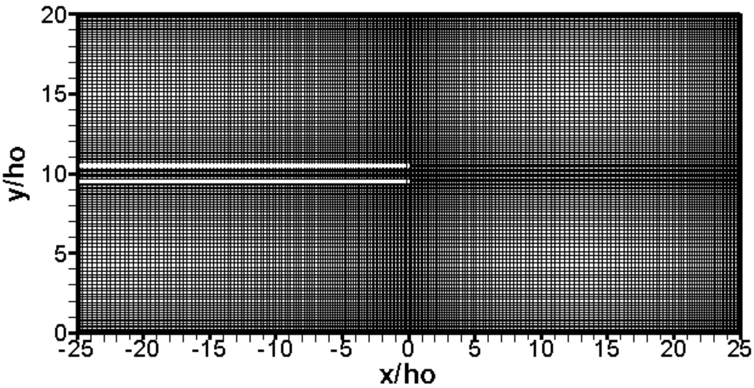

Figure 3: Typical grid of the jet–cavity interaction.

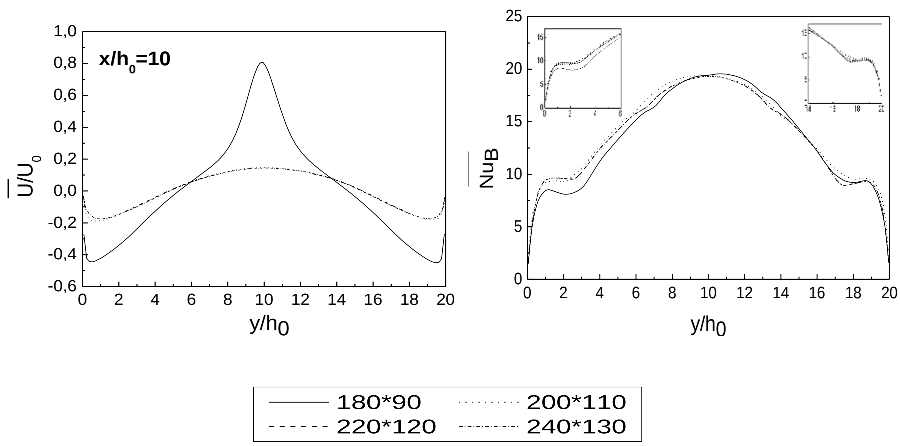

Figure 4: Effect of grid refinement for (L_f =25and L_h=10) and Re =4000.

achieved at 220 $\times$ 120 distributions beyond which no further significant change in average Nusselt number distribution and the average axial mean velocity is noticed. The grid independence tests are checked for each jet-cavity interaction. Additionally, the influence of the time step is also deepened. Knowing that the frequencies of oscillation of jet flapping are relatively low, a first order time scheme is achieved for time interpolation. For each case, the courant number is about unity in for the most part of the flow field.

3 Results and discussion

3.1 Flow field

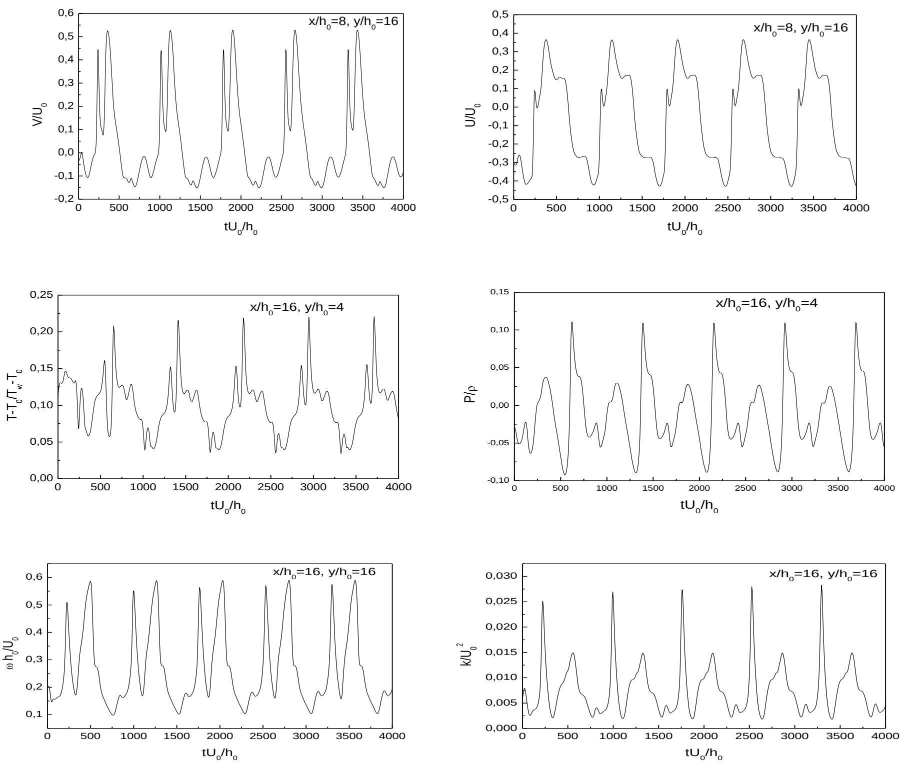

Figure 5: Computed dimensionless time evolution of the mean velocity components, pressure, temperature, kinetic energy and specific dissipation rate, for jet exit location (L_h=10, L_f=30) and Re=4000.

In this paper we consider a rectangular hot cavity with its one end open to the ambient air (fig.1). The jet exits from a rectangular duct inside the cavity. The jet exit location can be varied in order to investigate the effect of the lateral wall L_h and the bottom wall L_f. For a given jet location inside the cavity (L_h=10 L_f=30), figure 5 confirms the periodic behavior of dimensionless time-averaged of each variable: the mean velocity components, the mean pressure, the mean temperature, the kinetic energy and specific dissipation. So, the oscillation of the jet is evidenced numerically. For a given Reynolds number, the period of the oscillation is analogous at all point of the configuration. For several jet location within the oscillatory zone [Mataoui et al. (2001)], other test are investigated to detect the corresponding jet flapping frequency.

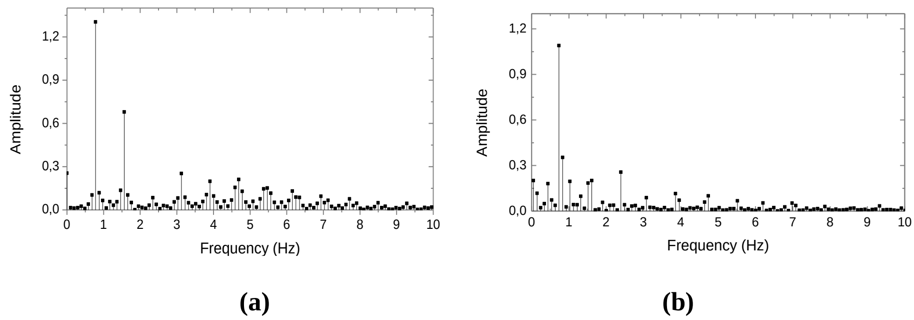

Figure 6: Fourier modes for U-velocity (a) and V-velocity (b) Jet exit location (L_f =30, L_h=10) , (x/h_0=8, y/h_0=16) and Re = 4000.

As example, Figure 6 shows the Fourier transforms of the velocity components time signals at the same point (x/h_0=8, y/h_0=16). The fundamental frequency is clearly determined by the first peak of the Fourier modes distribution. The frequency versus the impinging distance of the jet exit (L_f) for two heights (L_h) of the jet exit is illustrated in figure 7. For these two cases, the frequency increases moderately with the horizontal impinging distance (L_f). The predictions from the *(k-ω)* model are in good overall agreement with the experimental measurements of Mataoui et al. (2001).

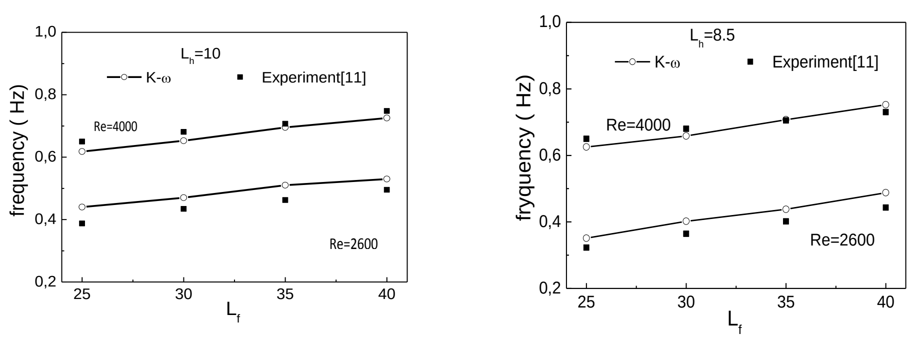

Figure 7: Frequency of oscillation for versus impingement distance L_f.

Figure 8 shows during one period of oscillation, the experimental visualization of Mataoui et al. (2001) and the corresponding values of the vorticity magnitude contours and the streamlines contours ; for Reynolds number of Re = 4000 and the jet exit location of L_h=8.5, L_f=40. Qualitatively, good agreement is obtained between the two predictions. The jet in the cavity generates the development of two counter rotating eddies on each side of the jet. These two eddies are evidenced by the calculated streamlines contours, also some secondary eddies appear in the cavity corners.

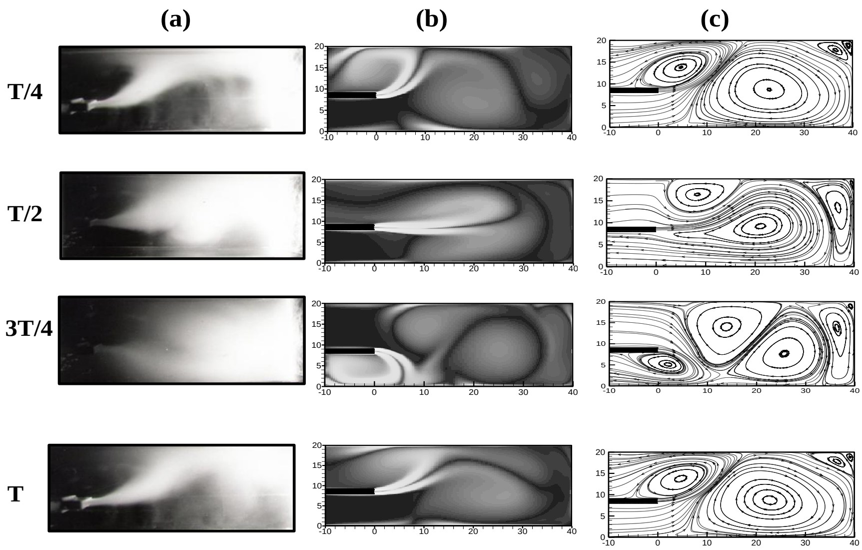

Figure 8: Flow structure (a) experimental flow visualization, (b) the magnitude of the vorticity and (c) streamlines contours each quarter of a period of oscillation Re=4000, L_h=8.5, L_f=40).

The oscillatory phenomenon is due to the instability generated by the pattern of a jet flowing between two eddies. So, the self-sustained oscillations are produced by the periodic deflection of the jet axis due to the Coanda effect [Shakouchi (1989); Mataoui, schiestel (2009)]. Contrary, the case of the axisymmetric jet flowing in a cylindrical cavity remains steady [Zidouni et al. (2009); Hallouane et al. (2013)].

These contours confirm that the interaction of the jet into the cavity produces two counter rotating eddies on each side of the jet, responsible of the oscillatory phenomenon. Within one period of time. The clockwise vortex on the upper side of the jet becomes larger and the counterclockwise vortex on the down side disappears because of negative wall shear stress, progressively. A new small clockwise vortex appears near each cavity corner. Once the jet axis deflects from its horizontal position, the eddies begin to move by varying their sizes. The largest eddy from the unattached side is driven upstream generating a pressure drop as it approaches the lateral exit; at the same time the fluid is sucked inside the cavity towards the opposite side, increasing the corresponding eddy size which is pushed downstream and forces the jet to deflect until to attach to the opposite side, where a maximum pressure occurs. The pressure within the two main laterals eddies periodically varies inducing the deflection of the jet. Hence the jet leaves from one side wall to the opposite one. The same phenomenon is repeated periodically. These mechanisms of oscillatory motion are quite identical with the observations of Mataoui et al. (2001) for similar parameter of flow interaction.

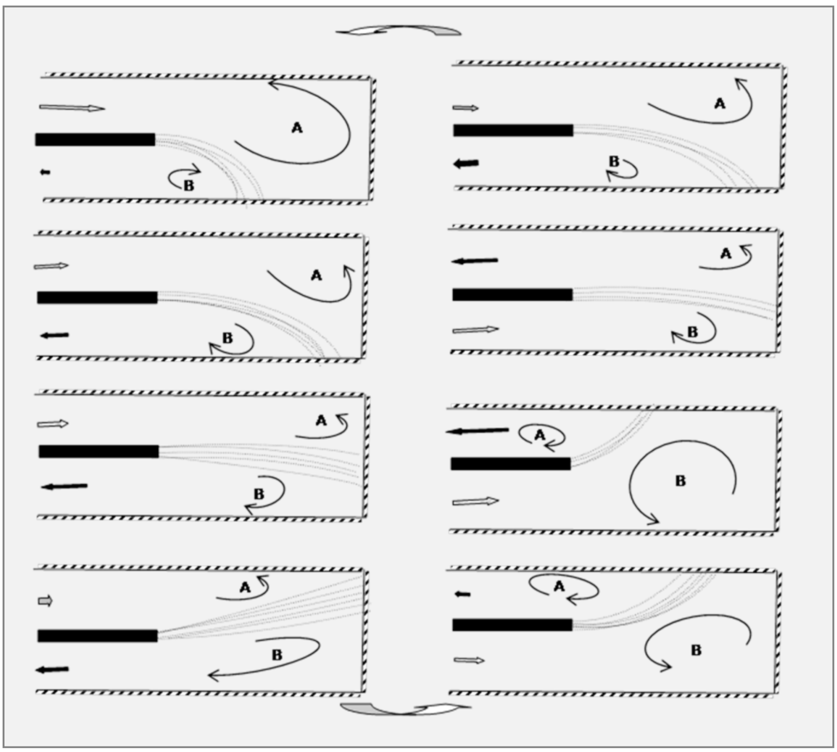

Figure 9: Sketch of oscillation mechanism.

The oscillation mechanism is sketched schematically in Figure 9. This figure shows 08 stages of one period of time. This figure indicates the rotation of the vortices, and the flow direction at the upper and lower exits. The intensity of these aspirations and fluid outlet is indicated qualitatively by the magnitude and the direction of the corresponding arrow.

3.2 Heat transfer

For the thermal study, the variation of instantaneous local Nusselt number along the three walls of the cavity during one period of time, for the case L_f=30 and L_h=8.5 , Re=5000 are illustrated in figure10. The local Nusselt number varies with time and positio; it was calculated from the temperature gradient at the hot plate as:

$$Nu(t,n) = -\left(\frac{h_0}{T_H - T_c}\right)\left(\frac{\partial T}{\partial n}\right)_{mwall} \tag{8}$$

Where *n* is the perpendicular direction to the corresponding wall.

In this figure the streamlines contours justify the Nusselt number variation, particularly the stagnation point location where the jet attaches the wall. The deflection of the jet induces unlike local Nusselt number distribution on the each cavity wall. Since the heat transfer rate is closely related to the flow pattern behavior. It is observed from these figures that at each times, there is some peak of local Nusselt number at the corresponding stagnation points. At the outlet boundary another maximum is observed, where pressure outlet boundary condition is specified, inducing a shear driven backflow; the code imposes at this boundary a reference temperature of the incoming flow (ambient temperature). This process is non-physical. However, this effect is only local and has little influence in the flow and thermal fields.

The location of the Nusselt number overshoots varies versus the time as follows:

At t_1 the local Nusselt number along the cavity bottom is higher value than that of the upper and lower lateral walls. This is due to the impingement of the principal jet on the cavity bottom where the heat transfer is greater. The local Nusselt number of the upper wall Nu_L represents reaches a maximum value at the entry of the cavity due to the aspiration of ambient air.

At t_2 and t_3 the jet impinges the upper wall which causes a greater heat transfer at this face compared with the cavity bottom and lower walls.

At t_4, t_5 and t_6, the inverse observations are obtained.

However the visual analysis of this figure shows that, when the flow should impinges directly the corresponding wall where the transfer is maximum and in the case where the jet changes its direction, the heat transfer decreases. Therefore, the local Nusselt number closely follows instantaneously the flow behavior.

To examine the effect of jet location and Reynolds number, on the overall flow and heat transfer process, the instantaneous variation of the average Nusselt number at each cavity wall is deduced by integrating it over the length of the corresponding

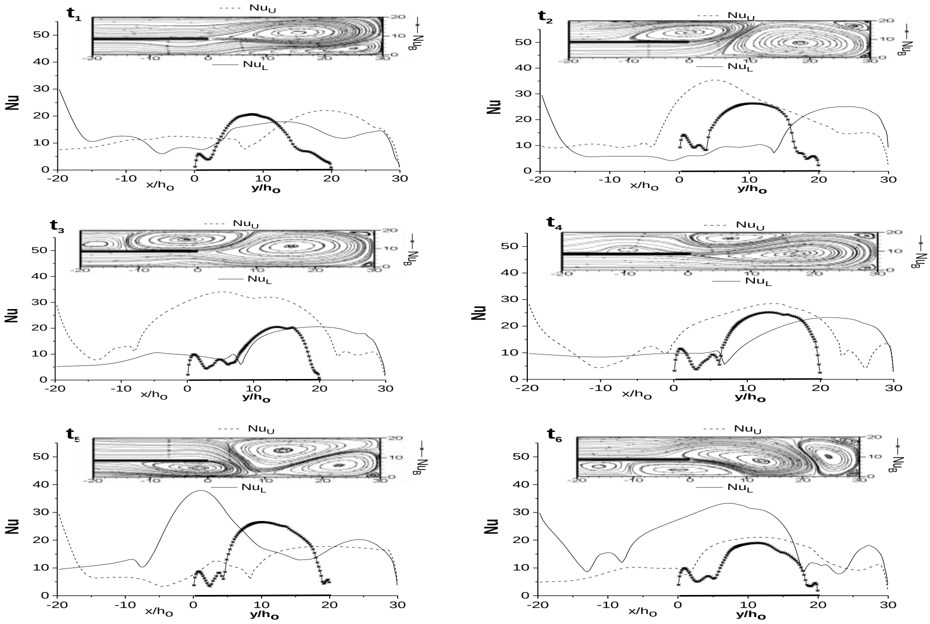

Figure 10: The stream lines and the local Nusselt number for the three walls of the cavity at each quarter period T. L_f=30 and L_h=8.5, Re=5000.

wall, as follows:

$$Nu_{avr}(t) = \frac{1}{L}\int_0^L Nu(t,n)dn \tag{9}$$

Where n is the direction to the corresponding wall

As shows figure 11, the time averaged Nusselt number varies periodically in time for all the cases analyzed in this study.

For the symmetrical interaction (L_h=10), fig11(a) shows the variations of the average Nusselt number of the upper and lower lateral cavity walls. Similar trend is obtained for all horizontal impinging distance (L_f). Moreover, average Nusselt number of the upper and lower walls are fully coupled: a maximum peak of Nu_u corresponds to a minimum value for the Nu_L and vice versa. The two signals are in opposite phases. On the other hand, the Nusselt number on bottom Nu_B is closely related to the horizontal impinging distance L_f, when L_f decreased Nu_B increases. However, the shape of the instantaneous signals of Nu_B is completely different due to the symmetrical flapping motion of the jet (for one period the jet impinges the

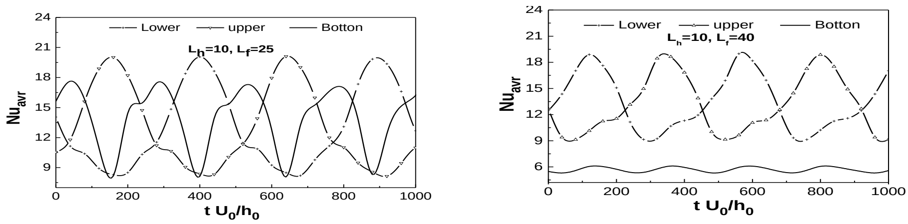

(a)

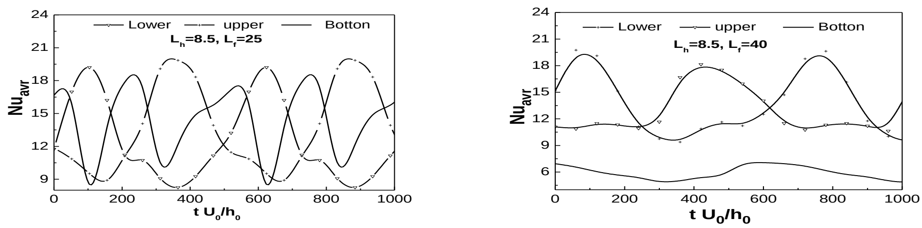

(b)

Figure 11: Average Nusselt number of the three walls of the cavity Re=4000.

bottom twice), the frequency of the signal looks to be around double the true frequency of the phenomenon.

For asymmetrical interaction (L_h=8.5) (fig 11-b), the Nusselt number Nu_L and Nu_u are in opposite phase. The double frequency of the signal of the Nusselt number of the bottom Nu_B despairs when L_f increased.

The effect of the Reynolds number on the instantaneous variation of the average Nusselt number (Nu_U, Nu_L, Nu_B) is given in fig. 12. It can be observed from this figure, that increasing Reynolds number enhances heat transfer for the three walls of the cavity. Furthermore, when Reynolds number increases the frequency of oscillation increases. This result reproduces the available experimental data of Mataoui et al. (2001)

For symmetric case, the average Nusselt number along the cavity walls is plotted from the distance of the jet exit to the bottom wall (impinging distance L_f) for several values of Reynolds number (figure 13).The average Nusselt number is deduced by:

$$\overline{Nu} = \frac{1}{T}\frac{1}{L}\int_0^T\int_0^L Nu(t,n)dndt \tag{10}$$

From Fig. 13a, the average Nusselt number on bottom wall decreases with horizontal impinging distance (L_f). This can be explained by the effect of the confinement.

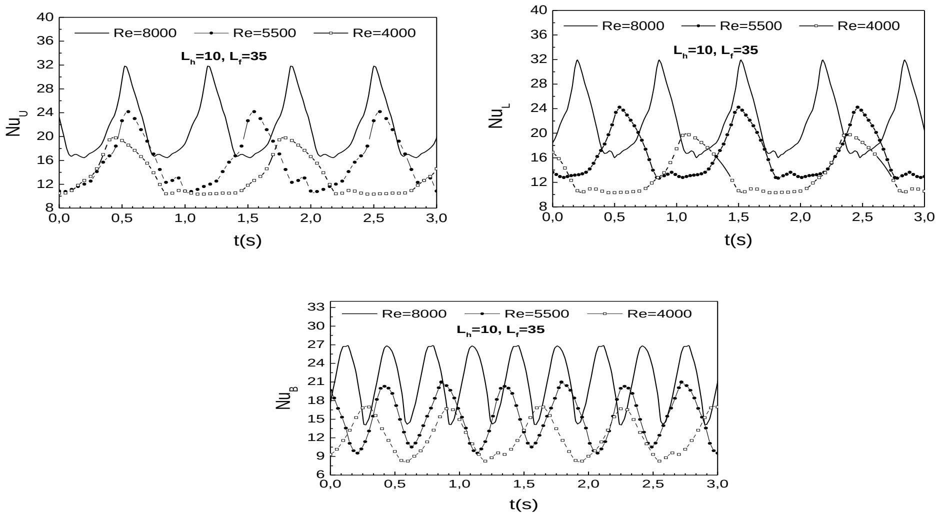

Figure 12: Influence Reynold number on the average Nusselt number for the three walls of the cavity.

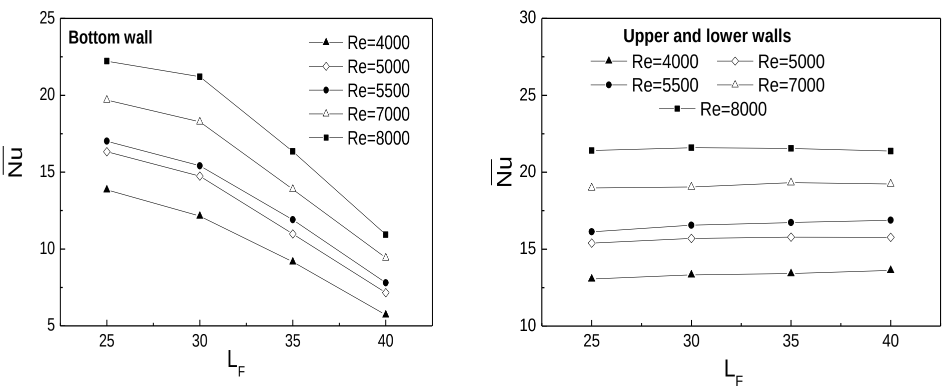

(a) (b)

Figure 13: Effect of impinging distance on mean Nusselt number for the cavity walls.

When the distance between the jet and the bottom becomes larger, the jet hits the bottom lower velocity. Almost no enhancement on heat transfer can be found on the upper and lower wall when L_f increases (Fig. 13b) .

The average Nusselt number along the walls that form the cavity is deduced from eq. 11:

$$\overline{Nu}_{cavity} = \overline{Nu}_{bottom} + \overline{Nu}_{upper\,lateral\,wall} + \overline{Nu}_{Lower\,lateral\,wall} \quad (11)$$

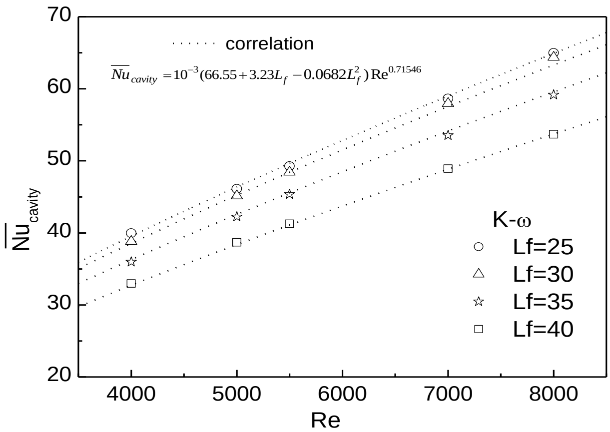

Figure 14: Mean Nusselt number distribution with Reynolds number.

For the symmetrical case the average Nusselt numbers $\overline{Nu}_{cavity}$ are correlated with jet Reynolds number and nozzle–to-bottom wall distance L_f , following the curve fitting technique using least-squares method as shown in Fig. 14. The suggested correlation of the present study is in good agreement with the computed values of average Nusselt number with an accuracy inferior 2% .

$$\overline{Nu}_{cavity} = 10^{-3}(66.55 + 3.23L_f - 0.0682L_f^2)Re^{0.71546} \quad (12)$$

4 Conclusion

A comprehensive numerical simulation for the forced convection heat transfer of a slot jet impinging a hot rectangular cavity is examined in this work using one point closure turbulence model. Depending on the location of the jet exit inside the cavity several flow regimes occur. In this paper, we have focused on the heat transfer self-oscillation phenomenon. The comparison of the flow structure by the present simulation with experimental results shows a good agreement is obtained qualitative and quantitative. For a given jet location inside the cavity, all variables have a periodic behavior versus time with the same frequency. Deflection of the jet is verified numerically by the instantaneous streamline contours within a period of time.

Due to the self-oscillation of the jet, the three walls of the cavity are cooled simultaneously. The heat transfer along the cavity walls is also periodic and depends on the variation of the size of the eddy in the time.

The numerical results show that the time-averaged Nusselt is also periodic and depends on the Reynolds number and the jet location inside the cavity (L_F, L_h). For the symmetrical case, the evolution of average Nusselt number is correlated according to the impinging distance and Reynolds number $\overline{Nu} = f(L_f, Re)$.

References

Amon, C. H.; Majumdar, D.; Herman, C. V.; Myinger, F.; mikic, B. B.; Sekulic, P. (1992): Numerical and experiment studies of selft-sustained oscillatory flows in communicating channels. *Int.J.Heat Mass Transfer*, vol. 35, no. 11, pp. 3115-3129.

ANSYS FLUENT 14.0 *CFD* code Documentation.

Benmouhoub, D.; Mataoui, A. (2013): Computation of heat transfer of a plane turbulent jet impinging a moving plate. *thermal science*.

Brignoni, L. A.; Garimella, S. V. (2000): Effect of Nozzle Inlet Chamfering on Pressure and Heat Transfer in Confined Air Jet Impingement. *Int. Journal of Heat and Mass Transfer*, vol. 43, pp. 1133-1139.

Chan, T. L.; Leung, C. W.; Jambunathan, K.; Ashforth-Frost, Y. S.; Zhou, Y.; Liu, M. H. (2002): Heat transfer characteristics of a slot jet impinging on a semi-circular convex surface. *Int.J. Heat Mass Transfer,* vol. 45, pp. 993-1006.

Halouane, Y.; Mataoui, A.; Iachachene, F. (2013): Turbulent heat transfer for impinging jet flowing inside a cylindrical hot cavity, thermal science.

Kim, A. (2012): Numerical study on heat transfer in laminar pulsed slot jets impinging on a surface. *World Academy of Science, Engineering and Technology,* vol. 69, pp. 479-476.

Li, P. W.; Tao, W. Q. (1993): Numerical and experimental investigations on heat/mass transfer ofslot-jet impingement in a rectangular cavity. *Int. J. Heat and Fluid Flow,* vol. 14, no. 3, pp. 246-253.

Mahrouche, O.; Najam, M.; El Alami, M.; Faraji, M. (2013): Mixed Convection Investigation in an Opened Partitioned Heated Cavity. *Fluid Dyn. Mater.Process*, vol. 9, no. 3, pp. 235-250.

Martin, H. (1977) :Heat and mass transfer between impinging gas jets and solid surfaces. *Advances in Heat Transfer*, 13, Academic Press, New York, pp. 1–60.

Mataoui, A.; Schiestel, R.; Salem, A. (2001): Flow Regimes of Interaction of a Turbulent Plane Jet Into a Rectangular Cavity :Experimental Approach and Numerical Modelling. *Journal of Flow, Turbulence and Combustion*, vol . 67, no. 1, pp. 267-304.

Mataoui, A.; Schiestel, R. (2009): Unsteady phenomena of an oscillating turbulent jet flow inside a cavity: Effect of aspect ratio. *Journal of Fluids and Structures*, vol. 25, pp 60–79.

Menter, F. R. (1994): Two-Equation Eddy-Viscosity Turbulence Models for Engineering Applications. *AIAA Journal*, vol. 32, no. 8, pp. 1598-1605.

Ogab, A. (1985): Contribution a L'étude de L'évolution d'un Jet Plan Turbulent dans une Cavité de Section Rectangulaire, Thèse De Magister*, Mécanique Des Fluides, Usthb Alger.*

Patankar, S. V. (1980): Numerical heat transfer and fluid flow, Series in computational methods in mechanics and thermal sciences, *hemisphere Publiching Corporation*.

Shakouchi, T. (1989): a New Fluidic Oscillator, Flowmeter, Without Control Port and Feedback Loop. *J. Dyn. Syst. Measur. Control*, vol. 111, pp. 535–539 .

Shakouchi, T.; Kuzuhara, S.; Yamaguchi, J. (1986): Oscillatory Phenomena of an Attached Jet. *Bull. Jsme,* vol. 29, pp. 1117–1123.

Valencia, A. (1999): Heat transfer enhancement due to self-sustained oscillating transverse vortices in channels with periodically mounted rectangular bars. *International Journal of Heat and Mass Transfer*, vol. 42, pp. 2053-2062.

Wilcox, D. C. (1994): Turbulence Modelling for CFD. *DCW Industries Inc*, La Canada, CA.

Zidouni–Kendil, F.; Mataoui, A.; Benaissa, A. (2009): Flow Structures of a Round Jet Evolving Into a Cylindrical Cavity. *International Journal of Transport Phenomena*, vol. 11, no. 2, pp. 165-183.